ISSN: 2454-9940

INTERNATIONAL JOURNAL OF APPLIED SCIENCE ENGINEERING AND MANAGEMENT

E-Mail :
editor.ijasem@gmail.com
editor@ijasem.org

www.ijasem.org

INTERNATIONAL JOURNAL OF APPLIED SCIENCE ENGINEERING AND MANAGEMENT

ISSN:2454-9940
www.ijsem.org
Vol 14, Issuse.3 Aug 2023

LEAD ZIRCONATE TITANATE NANOCERAMICS AND THE IMPACT OF SR DROPING ON THEIR ELECTRICAL CHARACTERISTICS

V N V RADHA KRISHNA MURTY[1] , KIRAN BACHINA [1]

ABSTRACT

Sol-gel synthesis was used to create Pb1-xSrxZr0.52Ti0.48O3 (PSZT) with x D = 0- 10% by mole. Crystals have both rhombohedral and tetragonal symmetry, as seen by the X-ray diffraction (XRD) patterns. Stacking in a lattice Strain, dielectric constant, and piezoelectric coefficient (d33) are all improved by the addition of Sr.PSZT's relaxation period increases from 106 (106 seconds) at 10 mol percent to 107 (107 seconds) at higher temperatures. A rise from 0.21 (0.05) to 0.26 (0.05) may be seen in the spreading factor. For materials at a 10% concentration, the coercive electric field was 15.97 kV/cm and the maximum residual electric polarization was 13.64 mC/cm2.

KEYWORDS:*Synonyms: PSZT, nanocrystalline, ferroelectric, piezoelectric*

Introduction

Lead zirconate titanate (PZT) is an example of a ceramic that contains ABO3. Due to the inclusion of lead zirconate (PbZrO3) and lead titanate (PbTiO3), this compound has both ferroelectric and anti-ferroelectric properties [1]. PZT's Para to ferroelectricity changes with temperature. For a variety of technological applications, its high Curie temperature (Tc) is a desirable quality. There is a lot of sensitivity in the crystal structure to the Zr/Ti ratio. Zr-rich PZT crystallizes into rhombohedra, whereas Ti-rich PZT crystallizes into tetragons

ASSOCIATE PROFESSOR [1,]
Mail id : radhakrishnamurthy.vnv@bvricedegree.edu.in
HOD & ASSOCIATE PROFESSOR [2],
MAIL Id: kiran.b@bvricedegree.edu.in
B V RAJU COLLEGE, BHIMAVARAM

ISSN:2454-9940
www.ijsem.org
Vol 14, Issuse.3 Aug 2023

The morphotropic phase boundary (MPB; Zr/Ti » 52/48; see also [2]) is the dividing line between the rhombohedra and piezoelectric properties, MPB has great potential as a technological material. Uses for the Zr/Ti « 52/48 composition range from sensors and actuators to non-volatile memory and transducers [3-5]. The final properties of PZT may be significantly impacted by both the atoms used to fill the Pb and Zr/Ti sites and the production procedure. Donor doping, acceptor doping, and isovalent doping are the three different substitution types that may occur when an element is doped. When the doped element has a negative charge relative to the host cation in hard PZT, oxygen vacancies form, leading to diminished electrical characteristics, an asymmetric hysteresis loop, and a robust coercive field [6, 7]. To make PZT more pliable, lead vacancies may be introduced by replacing the host metal with one that has a higher positive charge. This material is exceptional due to its small coercive field, high electrical conductivity, and symmetric hysteresis loop [8-12]. When the original action is substituted with an action that has the same charge as the host cation, however, charge neutrality is maintained. When lead is released into the air, oxygen levels drop temporarily [13, 14]. Sr content of strontium-substituted PZT has been investigated in a number of research [13-18].

The tiny size of strontium elongates the lattice [15]. Nasar et al. [16] looked at how adding strontium to PZT changed its atomic structure. The piezoelectricity of PZT is improved by adding strontium [17, 18].

Due to strontium's fluxing activity during sintering, it is possible to utilize isovalent sputtering to replace lead with strontium, which improves density and, by extension, electrical properties. In order to get maximum conductivity, oxygen vacancy availability must be present. The way in which the dipole relaxation is affected by this replacement is intriguing.

tetragonal crystal phases. Due to its dielectric, ferroelectric, and

Research into Sr-doped PZT has mostly focused on its electrical and piezoelectric properties because to the high level of interest in its physics and prospective applications.

Experimental

The sol-gel method was used to synthesis Pb1-xSrxZr0.52Ti0.48O3, with x D = 0-10 mole%. They made use of an alokoxide precursor. Precursors such acetyl acetone, zirconium (IV) isopropoxide, strontium (IV) acetate, nitric acid, and zirconium (IV) isopropoxide were helpful. The powder was claimed at 700 degrees Fahrenheit and took three hours. Using hydraulic pressure, the claimed powders and a binder (Poly vinyl alcohol (PVA)) were compressed into pellets 1 mm thick and 10 mm in diameter. During the three hours it was heated to 1100 degrees Celsius, it got sintered. The pellets are electroplated with a silver paste. Calcined powder samples were analyzed by X-ray diffraction (XRD) at a scan rate of 2°C per minute from 20°C to 70°C using CuKa radiation (D 1.5405A _). An N4L LCR meter (PSM 1735) was used to determine the dielectric constant. Between 35.0 and 450.0 degrees Celsius and 102.0 and 106.0 hertz, the dielectric constant was determined. While being poling (in silicon oil), the samples were subjected to many poling fields at a very high temperature (»1208C). We investigated the P-E hysteresis loop of Pb1-xSrx Zr0.52Ti0.48O3 (PSZT) pellets at room temperature using a state-of-the-art hysteresis device. A SINOCERA YE2730Ad33 meter was used

INTERNATIONAL JOURNAL OF APPLIED SCIENCE ENGINEERING AND MANAGEMENT

ISSN:2454-9940
www.ijsem.org
Vol 14, Issuse.3 Aug 2023

to measure the ambient piezoelectric co-efficient (d33) of the poled pellet.

Results and Discussion

Pb1-xSrxZr0.52Ti0.48O3 powder X-ray diffraction patterns are shown in Figure 1 for x D = 0-10 mole%. The two closest matches to the observed peak are PDF No. 11-070-4060 and JSPDS No. b01-073-2022, both of which can be found in the ICDD database. The rhombohedral (R3m) and tetragonal (P4mm) symmetry indices of each peak have been determined. To calculate the FWHM of the XRD peak, a Gaussian fit was utilized. A average crystallite's size was calculated by

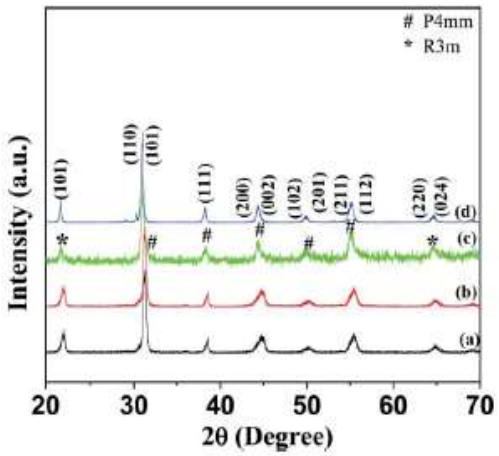

Figure 1. Pb1-xSrxZr0.52Ti0.48O3 X-ray diffraction (XRD) patterns, with (a) x D 0.02, (b) x D 0.04, (c) x D 0.06, and (d) x D 0.10.

The formula for Scherer is given in [19]. The crystals' performance was measured in nanometers. Smaller crystallites form when the Sr concentration is increased in the same synthetic environment (table 1). This is due to the fact that Sr has a smaller ionic radius (0.132 a _) than Pb (0.149 a _). The diffraction angle decreases with increasing strontium content. Table 1 shows that when Sr concentration rises, so does the lattice parameter.

Figure 2 is a scanning electron micrograph (SEM) of a pellet that was sintered at 1100_ C. Incorporating strontium into a material reduces the grain size and softens any rough edges. Micrometer- and nanometer-sized crystallites and grains are revealed by X-ray diffraction examination. That's why it's best to do experiments on polycrystalline samples.

Figure 3 shows the variation of the real part of the dielectric constant with temperature for Pb0.90Sr0.10Zr0.52Ti0.48O3. PZT materials are distinguished by their dielectric dispersion. The fall is sharp up to 1 kHz, flattens out beyond that, and then starts to reverse at extremely high frequencies. Ionic, orientation, space charge, and grain boundary polarizations may all contribute to a high dielectric constant at low frequencies. The effects of ionic and orientation polarizations are minimal at very high frequencies.

Table 1. Pb1-xSrx Zr0.52 Ti0.48O3 lattice parameters (a, b, c) for x D = 0.02, 0.04, 0.06, and 0.10. Inaccuracies are indicated with brackets.

	Rhombohedral	Tetragonal		
$Pb_{1-x}Sr_xZr_{0.52}Ti_{0.48}O_3$	a = b = c (nm)	a = b (nm)	c (nm)	Average crystallite size (nm)
x = 0.02	0.4086 (±0.0002)	0.4087 (±0.0001)	0.4093 (±0.0004)	33
x = 0.04	0.4076 (±0.0005)	0.4053 (±0.0003)	0.4076 (±0.0002)	30
x = 0.06	0.4047 (±0.0004)	0.4049 (±0.0007)	0.4054 (±0.0009)	23
x = 0.10	0.4035 (±0.0001)	0.4042 (±0.0002)	0.4050 (±0.0005)	20

INTERNATIONAL JOURNAL OF APPLIED SCIENCE ENGINEERING AND MANAGEMENT

ISSN:2454-9940
www.ijsem.org
Vol 14, Issuse.3 Aug 2023

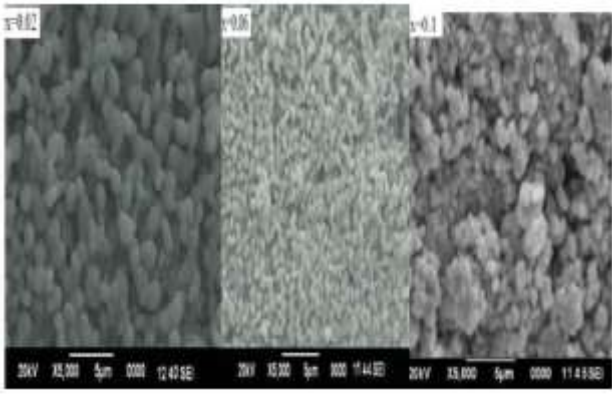

Figure 2. Samples sintered at 1100_C revealing the microstructure of Pb1-x Srx Zr0.52Ti0.48 O3 for x D = 0.02, 0.06, and 0.10.

The value or constant of the dielectric. To determine how much different ions contribute to the overall relaxing process, the Modified Debye's function was used.

$$\varepsilon' = \varepsilon'_{\infty} + \frac{\varepsilon'_{0} - \varepsilon'_{\infty}}{\left[1 + (\omega\tau)^{2(1-\alpha)}\right]} \qquad (1)$$

where ε', ε'_{0} and ε'_{∞} We provide you the low-frequency (100 Hz) and high-frequency (10 MHz) dielectric constant measurements we took. If we replace f with the applied frequency, t with the relaxation time, and a with the dispersion factor of the observed relaxation times relative to the mean, we may express the angular frequency of a 1 V signal as vD2pf. The calculated relaxation time and spreading factor (a) are shown in Table 2. This suggests that the calming effect is caused by a synergy of ions. The dielectric constant is mostly determined by the spreading factor, which increases with temperature. Below Tc, the dielectric constant decreases, and the spreading factor decreases with it. As the temperature of a material increases, the number of charge carriers in it decreases below its critical temperature (Tc).

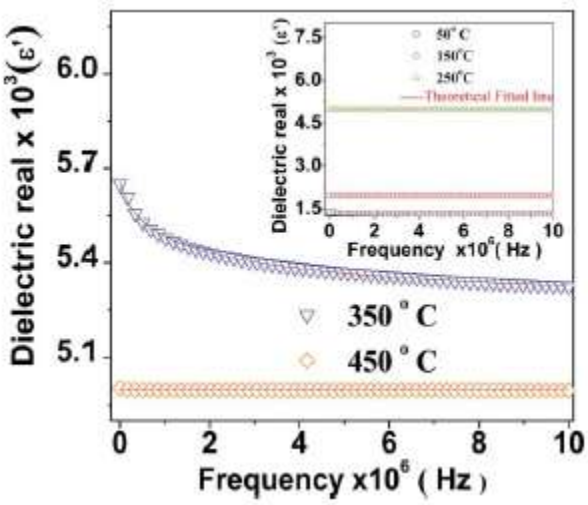

Figure 3. The true dielectric component of Pb0.90Sr0.10Zr0.52Ti0.48O3 as a function of frequency.

Table 2. Samples of Pb0.90Sr0.10 Zr0.52 Ti0.48O3 were measured at different temperatures, and the spreading factor (a) and relaxation time (s) were calculated using a model.

Temperature (°C)	Relaxation time (s)	Spreading factor (a)
50	2.1267E-06	0.20863
150	1.493E-06	0.24564
250	2.620E-07	0.28198
350	1.02E-07	0.27180
450	3.71E-7	0.26604

Has a dampening effect on the rate of spread. As shown by several publications [20, 21], the dielectric constant of the present-day samples changes as the temperature does. Each sample's ac conductivity was determined using the relation,

$$\sigma_{ac} = \omega\varepsilon_0\varepsilon_r\tan\delta \qquad (2)$$

The free-space permittivity, relative permittivity, and frequency are denoted by e0, err, and f, respectively, in this equation. Pb1-xSrxZr0.52Ti0.48O3 samples' ac

INTERNATIONAL JOURNAL OF APPLIED SCIENCE ENGINEERING AND MANAGEMENT

ISSN:2454-9940
www.ijsem.org
Vol 14, Issuse.3 Aug 2023

conductivity below the Curie temperature (at 275_C) is seen in Figure 4. These values represent x D = 2%, 6%, and 10% mole. The middle of the curve may be used to divide it in two. As a result of the activation-induced dispersion of ionic charge carriers, DC conductivity exhibits a low-frequency plateau. Jonscher's power-law analysis of the data points may shed light on the graph's high-frequency dispersion.

$$\sigma(\omega) = \sigma_0 + A\omega^n \quad (3)$$

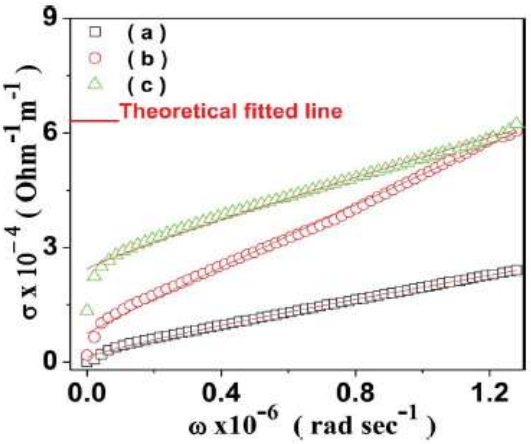

Figure 4. Pb1-xSrxZr0.52Ti0.48O3 ac conductivity at 2758C varies as a function of (a) x D 0.02, (b) x D 0.06 and (c x D 0.10.

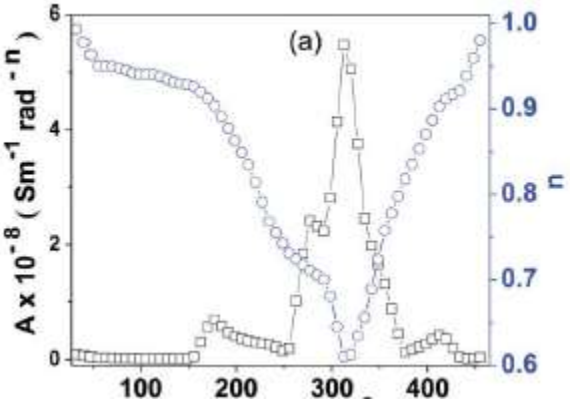

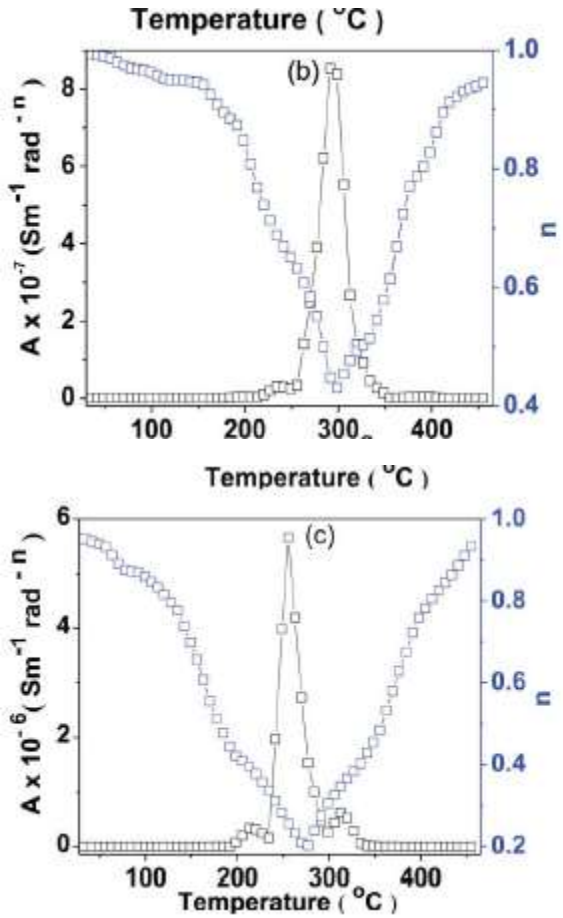

Figure 5. Temperature dependence of A and n in Pb1-x Srx Zr0.52 Ti0.48 O3 at (a)x D = 0.02, (b)x D = 0.06, and (c)x D = 0.10.

Zero represents the constant conductivity s0, a stands for the pre-exponential component that varies with temperature, and n stands for the frequency-dependent exponent. n may take on values between zero and one [22]. Figure 5 depicts the sensitivity of the A-to-n relationship to temperature. A, a ferroelectric parameter, increases with temperature.

A gets its highest value at the Curie temperature. The critical temperature for a par electric activity decreases with increasing a [23]. The frequency exponent n, defined in [24-26], characterizes the stability of the mobile ion-lattice interaction. Several mechanisms and their temperature

INTERNATIONAL JOURNAL OF APPLIED SCIENCE ENGINEERING AND MANAGEMENT

ISSN:2454-9940
www.ijsem.org
Vol 14, Issuse.3 Aug 2023

dependences are shown [27-31]. As dipole-dipole interactions are absent or very weak, n = 1, but as temperatures increase, n = 0, and

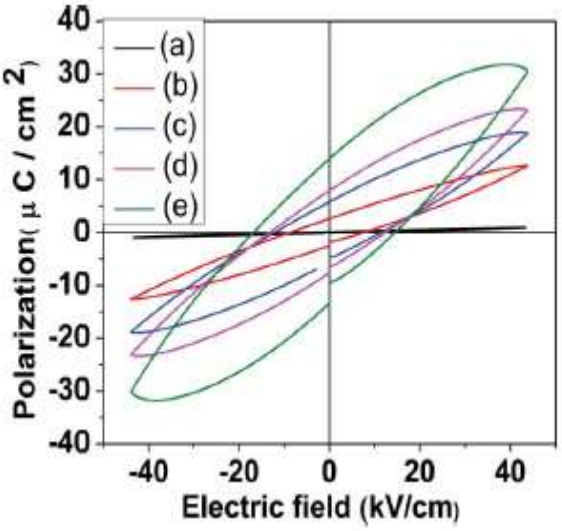

Figure 6. P-E diagram for Pb1-xSrxZr0.52Ti0.48O3 for various values of x D, from 0.00 in (a) to 0.06 in (e).

Heat, with very high temperatures being the norm. When the Curie temperature is the lowest possible. Oligomer large polaron tunneling (OLPT) is shown by the intersecting lines.

Figure 6 displays the power-efficiency (P-E) curves for Pb1-xSrxZr0.52Ti0.48O3 ceramics with x D = 0-10 mol%. As Sr concentration rises, the P-E loop enlarges. Table 3 displays the coercive fields and residual polarization of Sr-doped PZT. Ferroelectric polarization develops due to the ant symmetric atomic arrangement. An increase in polarization causes strain to partition the rhombohedral and tetragonal phases of PZT. The strain is increased when strontium (132A _) is used in place of lead (149A _). The residual polarization and coercive field are both improved by an increase in lattice strain.

Pb1-xSrxZr0.52Ti0.48O3 (x D 0-10 mole%) was tested in a variety of poling fields to determine its linear piezoelectric co-efficient (d33). Pb0.90Sr0.10Zr0.52Ti0.48O3, with a charge coefficient of 435 pC/N at 4.5 kV/cm (1 mol%, or x D 0.10), exhibits piezoelectric characteristics. When ferroelectric ceramics are polarized, their piezoelectric properties are activated. Both internal and external influences may have an impact on the piezoelectric behavior. When an electric field is applied to a ferroelectric material, a domain shift occurs. The lattice strain generates the intrinsic contribution. Increased piezoelectric activity results from ferroelectric domain alignment along the poling field direction. The ferroelectric characteristics of Sr-doped PZT were shown at the MPB.

Table 3. Remanent polarization (Pr) and coercive field (Ec) in Pb1-xSrx Zr0.52 Ti0.48O3 at x D = 0.00, 0.02, 0.04, 0.06, and 0.10.

$Pb_{1-x}Sr_xZ$ $_{0.52}Ti_{0.48}O_3$	Remnant polarization ($\mu C/cm^2$)	Coercive Field (kV/cm)
x = 0.00	0.11	4.74
x = 0.02	2.56	8.62
x = 0.04	5.26	12.01
x = 0.06	7.70	12.86
x = 0.10	13.64	15.97

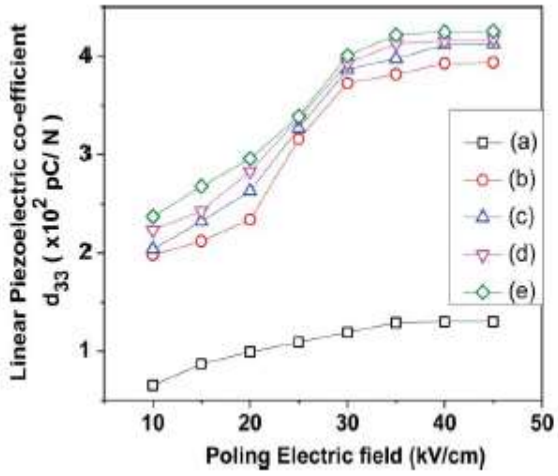

ISSN:2454-9940
www.ijsem.org
Vol 14, Issuse.3 Aug 2023

Figure 7. The linear piezoelectric co-efficient (d33) of Pb1-xSrxZr0.52Ti0.48O3 for different values of xD, from (a) xD = 0.00 to (e) xD = 0.10.

The free energy profile flattens during a structural phase transition. The ferroelectric state of nanocrystallite samples undergoes a symmetry change due to elastic clamping of the crystalline structure [31]. This has led to significant developments in piezoelectric characteristics.

Conclusion

$Pb_{1-x}Sr_xZr_{0.52}Ti_{0.48}O_3$ with x = 0.02, 0.04, 0.06 and 0.10

Create a crystal by combining rhombohedra and tetrahedra. To examine how charge carriers modify dielectric properties, a modified Debye's function is used. Large-scale polar tunneling superimposes itself over the conduction process, as seen by the ac conductivity. Sr doping enhanced ferroelectric and piezoelectric characteristics because of lattice strain.

References

1. M. E. Lines, A. M. Glass, Principle and Application of ferroelectrics and Related Materials. Clarndon. Oxford Press, (1977).

2. B. Jaffe, W. R. Cook, H. Jaffe, Piezoelectric ceramics. Academic press, London, (1971).

3. G. H. Haertling, Ferroelectric ceramics: History and technology, J. Am. Soc. 82, 797–818 (1999).

4. V. Koval, C. Alemany, J. Briancin, H. Brunckova, Dielectric properties and phase transition behavior of xPMN-(1-x) PZT ceramic systems, J. Electroceramics. 10, 19–29 (2003).

5. D. V. Taylor, D. Damjanovic, Piezoelectric properties of rhombohedral Pb[Zr,Ti]O3 thin film with (100), (111), and "random" crystallographic orientation, Appl Phys Lett. 76, 1615 (2000).

6. R. A. Eichel, P. Erhart, P. Traskelin, K. Albe, H. Kungl, M. J. Hoffmann, Defect-Dipole Formation in Copper-Doped PbTiO3 Ferroelectrics, Phys Rev Lett. 100, 095504 (2008).

7. S. C. Jung, H. B. Park, J. Kim, K. Kim, S. J. Kim, Structure and Electric Properties of PZT Ceramics Substituted by La and Nd, J Korean Ceram Soc. 31, 155–160 (1994).

8. S. Boonyen, L. Pdungsap, P. Winotai, T. Sudyoadsuk, P. Petchpong, Properties of gadoliniumdoped PZT (Zr:Ti D 52:48), Int J Mod Phys B. 16, 3515–25 (2002).

9. S. S. N. Bharadwaja, P. Victor, P. Venkateswaelu, S. B. Krupanidhi, ac transport studies of La-modified antiferroelectric lead zirconate thin films, Phys Rev B. 65, 174106 (2002).

10. F. Kulcsar, Electromechanical Properties of Lead Titanate Zirconate Ceramics with Lead Partially Replaced by Calcium or Strontium, Journal of the American Ceramic Society. 42, 49 (1959).

11. P. Kour, Pawan Kumar, S. K. Sinha, Manoranjan Kar, Study of dielectric and impedance spectroscopy of La substituted nanocrystalline Pb(Zr0.52Ti0.48)O3 ceramics, Journal of Materials Sciene: Materials in Electronics. 26, 1304–1310 (2014).

12. P. Kour, S. K. Pradhan, Pawan Kumar, S. K. Sinha, Manoranjan Kar, Enhanced ferroelectric and piezoelectric properties in La-modified PZT ceramics, Applied Physics A. 122, 591 (2016).

13. A. Dalakoti, A. Bandyopadhyay, S. Bose, Effect of Zn, Sr, and Y Addition on Electrical

ISSN:2454-9940
www.ijsem.org
Vol 14, Issuse.3 Aug 2023

Properties of PZT Thin Films, Journal of the American Ceramic Society. 89, 1140 (2006).

14. C. B. Sahoo, V. A. Jaleel, P. K. Panda, Development of PZT powders by wet chemical method and fabrication of multilayered stacks/actuators, Materials Science and Engineering B. 126, 80–85 (2006).

15. V. Kalem, I. Cam, M. Timucin, Dielectric and piezoelectric properties of PZT ceramics doped with strontium and lanthanum, Ceramics International. 37, 1265 (2011).

16. R. S. Nasar, M. Cerqueira, E. Longo, J. A. Varela, A. Beltran, Experimental and theoretical study of the ferroelectric and piezoelectric behavior of strontium-doped PZT, Journal of European Ceramics Society. 22, 209 (2009).

17. L. Kozielski, M. Adamczyk, J. Erhart, M. Pawelczyk, Application testing of Sr doping effect of PZT ceramics on the piezoelectric transformer gain and efficiency proposed for MEMS actuators driving, Journal of Electroceramics. 29, 133–138 (2012).

18. M. Khalid, M. Shoaib, A. A. Khan, Strontium doped lead zirconate titanate ceramics: study of calcinations and sintering process to improve piezo effect, J NanoSci Nanotechnol. 11, 5440 (2011).

19. B. D. Cullity, S. R. Stock, Elements of X-Ray Diffraction, Prentice-Hall Inc. (2001).

20. P. Kour, P. Kumar, S. K. Sinha, M. Kar, Effect of Strontium Substitution on dielectric constants of PZT Nanocrystalline Ceramics, AIP conf.Proc. 1536, 667 (2013).

21. P. Kour, P. Kumar, S. K. Sinha, M. Kar, Electrical properties of calcium modified PZT (52/48) ceramics, Solid State communications. 190, 33–39 (2014).

22. A. K. Jonscher, Dielectric Relaxation in Solids, Chelsea Dielectric Press, London, (1983).

23. R. Ranjan, R. Kumar, N. Kumar, B. Behera, R. N. P. Choudhary, Impedance and electric modulus analysis of Sm-modified Pb(Zr0.55Ti0.45)1-x/4O3 ceramics, J Alloys and Compounds 509, 6388–6394 (2011).

24. B. Patti, B. C. Sutar, B. N. Parida, P. R. Das, R. N. P. Choudhary, Pyroelectric and dielectric properties of lead-free ferroelectric Ba3Nb2O8 ceramic, J Mater Sci: Mater Electron 24, 1608–1616 (2013).

25. S. Saha, T. P. Sinha, Low-temperature scaling behavior of BaFe0.5Nb0.5O3, Phys Rev B. 65, 134103– 134106 (2002).

26. C. Leon, A. Rivera, A. Varez, J. Sanz, Santamaria, K. L. Nagi, Origin of constant loss in ionic conductors, Phys Rev Lett. 86, 1279–1282 (2001).

27. E. V. Gopalan, K. A. Malini, S. Saravanan, D. S. Kumar, Y. Yoshida, M. R. Anantharaman, Evidence for polaron conduction in nanostructured manganese ferrite, J Phys D Appl Phys 41, 185005–185014 (2008).

28. T. M. Meaz, S. M. Attia, A. M. Abo, El. Ata, Effect of tetravalent titanium ions substitution on the dielectric properties of Co-Zn ferrites, J Magn Mater 257, 296–305 (2003).

29. A. Ghosh, ac conduction in iron bismuthate glassy semiconductors, Phys Rev B 42, 1388–1393 (1990).

30. T. Kimura, T. Goto, H. Shintani, K. Ishizaka, T. Arima, Y. Tokura, Magnetic control of ferroelectric polarization, Nature. 426, 55–58 (2003).

ISSN:2454-9940
www.ijsem.org
Vol 14, Issuse.3 Aug 2023

31. A. G. Zembilgotov, N. A. Pertsev, R. Waser, Phase states of nanocrystallite ferroelectric ceramics and their dielectric properties, J Appl Phys. 97, 114315 (2005).